
Distributed Online Rollout for Multivehicle Routing in Unmapped Environments

Jamison Weber, Dhanush Giriyan, Devendra Parkar, Andréa Richa, Dimitri Bertsekas

School of Computing and Augmented Intelligence

Arizona State University

Tempe, USA

Email: {jwweber, dgiriyan, dparkar1, aricha, dbertsek}@asu.edu

Abstract

In this work we consider a generalization of the well known multivehicle routing problem: given a network, a set of agents occupying a subset of its nodes, and a set of tasks, we seek a minimum cost sequence of movements subject to the constraint that each task is visited by some agent at least once. The classical version of this problem assumes a central computational server that observes the entire state of the system perfectly and directs individual agents according to a centralized control scheme. In contrast, we assume that there is no centralized server and that each agent is an individual processor with no a priori knowledge of the underlying network (including task and agent locations). Moreover, our agents possess *strictly local communication and sensing capabilities* (restricted to a fixed radius around their respective locations), aligning more closely with several real-world multiagent applications. These restrictions introduce many challenges that are overcome through local information sharing and direct coordination between agents. We present a *fully distributed, online and scalable reinforcement learning algorithm* for this problem whereby agents self-organize into local clusters and independently apply a multiagent rollout scheme locally to each cluster. We demonstrate empirically via extensive simulations that there exists a critical sensing radius beyond which the distributed rollout algorithm begins to improve over a greedy base policy. This critical sensing radius grows proportionally to the \log^* function of the size of the network, and is therefore a small constant for any relevant network. Our decentralized reinforcement learning algorithm achieves approximately a factor of two cost improvement over the base policy for a range of radii bounded from below and above by two and three times the critical sensing radius, respectively. In addition, we observe in simulations that our distributed rollout algorithm requires exponentially fewer computational resources than the classic centralized approach, at only a small constant factor detriment in cost. Lastly, we validate our algorithm through physical robot experiments in continuous space, and show that the resulting behavior reflects what we observe in the discrete space simulations.

1 Introduction

There have been prolific recent advances in the field of distributed computing on engineering collective behavior for systems of agents. Such agents are typically restricted to only local computations and interactions with other agents to achieve a desired system-wide behavior, as in population protocols [4] and programmable matter [14, 12, 26, 24, 27]. Likewise, AI researchers have also considered multiagent problems wherein the full state is not directly observable to the agents, and for which proposed solutions require centralized computation—often executed offline [6, 11, 15, 18, 19].

A formulation known as a *decentralized partially observable Markov decision process* (Dec-POMDP) was introduced in [7] that combines these ideas, but optimally solving these was shown to be intractable. In these formulations, the environment is partially observable to each agent, but the information sensed by each agent is not universally shared. Approximate solutions to Dec-POMDPs were explored in [1, 3, 2], but ultimately relied on intensive offline and centralized simulations. As the state and control spaces increase in size, the computational cost of computing even approximately optimal policies can become prohibitively expensive in practical settings. On the other hand, fully distributed algorithms can be challenging to design, but invariably scale much more efficiently than systems that rely on centralized computation. This is primarily attributed to the parallelizability of local rules, which tend to be simple and come at low cost.

In this work, we consider a generalization of the well-studied multi-vehicle routing problem (MVRP). The MVRP involves a set of agents (vehicles) and a set of tasks each occupying a position on an underlying network on N nodes. The objective is to compute a sequence of movement decisions for each vehicle such that the total number of vehicle movements is minimized, subject to the constraint that each task is visited at least once by some agent. Classically, these sequences are computed by a centralized controller that has perfect access to all state information, and may freely direct all agents according to the control sequences it computes. Our generalization addresses scenarios where the network topology, including the positions of other agents and tasks, is not known a priori, and where each agent possesses sensing and inter-agent communication capabilities that are limited to a radius around its location on the network (e.g. as in radio networks). We refer to this as the Unmapped Multivehicle Routing Problem with Local Constraints (UMVRP-L). In this distributed setting, local communication between agents is necessary for coordination and information exchange.

The UMVRP-L is challenging for agent coordination algorithm design. Algorithmically, one may consider a reinforcement learning solution, but as the underlying network is unknown, methods that require offline computation such as Q-Learning [22], policy approximation (via the training of parametric architectures) [10], or executing policy iteration to near convergence [21] may not be applicable. This realization suggests rollout [9] as a natural candidate, as it is a reinforcement learning algorithm that admits a fully online solution when equipped with the appropriate heuristics, and produces reliably favorable results due to its fundamental connections to Newton’s method [8, 9].

The rollout algorithm requires a base policy, which provides a benchmark for comparison. This comparison allows us to analyze two fundamental concepts that arise in multiagent problems: *communication* and *coordination*. Communication refers to agents sharing sensed information, whereas coordination refers to agents organizing in such a way that they collectively solve a problem intelligently. We consider a greedy base policy whereby each agent moves toward the nearest “visible” task; hence the base policy requires neither communication nor coordination. On the other hand, rollout is a coordination scheme, although it typically assumes information is universally shared among agents. We examine the performance of rollout when communication is restricted to only local interactions within the sensing radius, and how this mandates distributed coordination and computation among the agents.

1.1 Our contributions

We present a full decentralization of a sequential method of control computation known as Multiagent Rollout [9], which we call Decentralized Multiagent Rollout (DMAR). In this approach, we assume each agent is an individual processor that executes DMAR—a distributed algorithm common to all agents—in parallel with other agents. DMAR uses simple local rules to induce iterative self-organization of the agent set into temporary local clusters of bounded size.

In one iteration of DMAR, agents that perceive tasks within their sensing radii become candidates for a cluster leader role that is associated with a specific region of the environment. A simple local leader election scheme then produces a single representative for each region, after which nearby agents iteratively join these respective clusters. The leader of each cluster initiates a message passing protocol to aggregate a map of the local region around the cluster gathered from the sensing data of the cluster agents. The leader then executes a sequential rollout scheme on the cluster, which produces a set control sequences (one for each agent in the cluster). This set is distributed to the corresponding agents via agent-to-agent message passing, after which each agent executes its corresponding sequence. Upon completion of all tasks in the cluster, cluster assignments systematically dissolve and this process repeats until all tasks have been completed globally. Note that these clusters do not necessarily

form a partition over the agent set, as isolated agents may not be assigned to a cluster. Agents that do not sense a task will attempt to locate tasks by randomly exploring the environment at the same time agents assigned to clusters coordinate and execute control schemes. On a global level, this yields a sequence of independent intra-cluster coordination schemes that aggregate to an approximate global solution, as we demonstrate experimentally. At a more granular level, agents proceed in synchronized time steps (see Sections 2,3).

We provide theoretical guarantees regarding the correctness of DMAR and show that each iteration terminates in constant time. Moreover, we conduct extensive discrete-space simulation results that compare the costs incurred by DMAR with those of a greedy base policy. In these experiments, we modulate the sensing radius over a wide variety of network topologies of various sizes, a variable number of tasks and multiple agent-to-task ratios. We demonstrate via extensive simulations that there exists a critical sensing radius beyond which DMAR begins to improve over a greedy base policy. This critical sensing radius grows proportionally to $\log_2^*(N)$,¹ and is therefore a small constant in practice regardless of the size of the network. Note that since $\log_2^*(N) \leq 5$ for any $N \leq 10^{10000}$, the size of any relevant network need not be known. Additionally, we consider an outer radius threshold whereby the radius becomes large enough that DMAR forms only a single cluster and therefore information is universally shared (as in MVRP). Our results further show that the performance of DMAR degrades gracefully from the outer radius down to the critical radius, demonstrating the effect on performance of limiting communication among agents. We show empirically that between these special radii, there is a range of *effective radii* bounded by $2\log_2^*(N)$ and $3\log_2^*(N)$ from below and above, respectively, whereby DMAR achieves approximately a factor of two relative cost improvement over the base policy on average. In this range, DMAR requires exponentially fewer computational resources as compared to the centralized multiagent rollout algorithm. Moreover, we observe that radii in this effective range incur a cost that is only a constant factor larger than those of the largest radii we considered in our experiments.

Lastly, we validate our algorithm through physical robot experiments in continuous space using the Robotarium platform [25] as a proof-of-concept. The resulting behavior reflects what we observe in discrete-space simulations, which demonstrates the algorithm’s robustness to sensor noise and underscores its real-world applicability. Potential applications of our algorithm are scenarios where it is not reasonable to assume that a complete mapping of tasks (and agents) exists. These include minefield disarmament [13], post-disaster search and rescue [17], and unmanned aerial vehicle navigation [5].

2 Model and preliminaries

An instance of the MVRP consists of a finite graph $G = (V, E)$ and a set S of m agents that occupy some initial subset of nodes. In addition, there is some subset τ of nodes that represent task locations. This model operates in discrete time advances, during which an agent may move to a node adjacent to its current location. Whenever an agent visits a task node, that task is considered *completed*, and is removed from the network. At each time step, a unit cost is incurred for each agent that moves from one node to an adjacent node. A solution Y is given by m sequences Y_1, \dots, Y_m of controls corresponding to each agent in S . We define the cost $C(Y)$ incurred by a solution Y as the sum of the lengths of the m control sequences, i.e. $C(Y) = \sum_{Y_i \in Y} |Y_i|$. A solution Y is optimal whenever $C(Y)$ is minimum. In this work, we consider regular, planar networks as discretizations of 2D space, although our algorithms can be extended to general graphs at a cost increase that is dependant on the maximum degree of the network. A subset of nodes representing obstacles in the network cannot be visited by agents. Note that MVRP is NP-Hard [23], even when the network is planar [16].

From a centralized perspective, the MVRP can be solved approximately in an online setting using *approximation in value space* [8]. That is, we approximate the *cost-to-go* elements of the Bellman equations via heuristics that can be computed online. In particular, we consider a greedy base policy; that is, each agent moves toward the nearest task visible to it. Denote Ω as the state space representing all possible agent and task configurations over G . Let $U_s(x)$ denote the set of m -dimensional control vectors permissible at state x_s and stage s . A stage dependent function $f : \Omega \times U_s \rightarrow \Omega$ defined as $f(x_s, u_s) = x_{s+1}$ describes the resulting state obtained from application of control u_s at state x_s .

$$^1\log_2^*(N) \stackrel{\text{def}}{=} \begin{cases} 0 & N \leq 1 \\ 1 + \log_2^*(\log_2(N)) & N > 1 \end{cases}$$

Lastly, denote $g(x_s, u_s)$ as the cost function indicating the total number of vehicle movements at stage s . Then the approximately optimal cost $\tilde{J}_s(x_s)$ of state x_s is given by

$$\tilde{J}_s(x_s) = \min_{u_s \in U_s(x)} \{g(x_s, u_s) + \tilde{J}_{s+1}(f(x_s, u_s))\}, \forall x_s \in \Omega \quad (1)$$

where $\tilde{J}_{s+1}(x_{s+1})$ refers to the cost-to-go obtained from simulation of a base policy.

Note that the minimization operation in Equation 1 is still exponential in m , however, a recent reformulation of a multiagent problem to an equivalent problem with a larger state space, but simpler control space was described by Bertsekas in [9]. This reformulation was the basis for substantial simplification of rollout and policy iteration algorithms for multiagent problems. The resulting algorithm (called *multiagent rollout*) dramatically reduces the computational complexity of each stage of the standard rollout algorithm (from exponential to linear in the number of agents), while maintaining its cost improvement properties. This exponential gain is achieved through sequential rollout control computation on an agent-by-agent basis, where each agent receives information computed by agents earlier in the sequence, hence greatly restricting the number of multi-component controls considered. Specifically, the control u_s^a for each agent a at stage s is computed in a sequence $u_s^{a_1}, u_s^{a_2}, \dots, u_s^{a_m}$, such that when $u_s^{a_i}$ is computed, each $u_s^{a_j}$ for $1 \leq j < i$ reflect a_j 's chosen control at stage s , and for any $u_s^{a_j}$ where $i < j \leq m$ and for all controls considered in future stages, a base policy is used to estimate the cost-to-go in Equation 1 via online simulation.

The UMVRP-L is a generalization of MVRP where G is not known a priori. Here we assume that each agent has some on-board computational capability and enforce that any computation must be executed by some agent, as opposed to a central controller. Moreover, there are *locality restrictions*, which we describe formally in this section. A solution and its corresponding cost to the UMVRP-L are defined analogously to the MVRP. An algorithm solves an instance of UMVRP-L correctly if all tasks are eventually completed without violating locality restrictions. We remark that the UMVRP-L is at least as difficult as MVRP since, in addition to visiting all tasks, agents must first locate them.

At a time step t , each agent a occupies some position $\rho_t(a) \in V$. A set $\rho_t(S') \subseteq V$ refers to a set of respective positions for an agent set $S' \subseteq S$ at time step t . For an agent a , we define the *view* of a at time step t , denoted as $\nu_t(a)$, to be the subgraph of G induced by $\rho_t(a)$ and all nodes reachable from $\rho_t(a)$ in at most k hops, where k is a radius parameter. An agent's view describes what it is able to sense from its location (i.e. obstacles, agents and tasks). As a view is determined by hops, agents may potentially "see" through objects. One may regard a view in terms of entire groups of agents. Let $S' \subseteq S$ be a set of agents. Then at time step t we denote $\nu_t(S') := \bigcup_{a \in S'} \nu_t(a)$, and refer to this as the *view* of an agent set S' at time t . For convenience, we may omit the subscript t if it is clear from the context.

A subset of agents confers a communication network where two agents form a communication link if and only if both stand in the intersection of their respective views. Algorithmically, agents may locally organize into special sets called *clusters*. A cluster K is a subset S' of agents associated with a *restricted communication network*, denoted as \mathcal{T}_K . Network \mathcal{T}_K is restricted in the sense that it forms a spanning tree over the full communication network over S' . We assume that each agent possesses a unique numerical ID and knowledge of a common small size parameter ψ ; a positive integer constant where $\mathcal{O}(2^\psi)$ bounds the diameter of an agent cluster from above (see Section 3). Agents also possess a single parent pointer, multiple child pointers (all initialized to NULL), and various boolean flags used for message passing.

In our distributed model we operate under *parallel synchronous (PS) time*. That is, in each discrete time step t , all agents are *activated* simultaneously in parallel, and thus may only act upon information communicated at time $t - 1$. As such, each agent is assumed to possess a *synchronized clock*. An agent *activation* may consist of either moving, performing some computation, or waiting. For an agent a , a computation performed by a may involve multiple full scans of $\nu_t(a)$, and any agent $b \in \nu_t(a)$ may have their memory modified directly by a .

3 Algorithms and analysis

In this section, we present and analyze a series of protocols that, when executed in sequence and repeated, will solve the UMVRP-L. We present a strictly local algorithm that allows us to apply multiagent rollout from [9] using a greedy shortest path heuristic that does not violate the

local constraints described in 2. We refer to the following sequence of protocols as **Decentralized Multiagent Rollout (DMAR)**. At the highest algorithmic view, agents collectively repeat the *phases* described in Algorithm 1 in sequence.

Algorithm 1 DMAR for UMVRP-L

repeat

1. Self-Organizing Agent Clusters (SOAC): Agents self-organize into clusters of size at most $\mathcal{O}(2^\psi)$ agents in local regions of the network. For each cluster K , locally form a tree \mathcal{T}_K , whose nodes represent agents.

2. Local Map Aggregation (LMA): For each cluster K , locally acquire the view held by each agent and route these subgraphs of G to the cluster leader (root of \mathcal{T}_K).

3. Team-Restricted Multiagent Rollout (TMAR): For each cluster K , the cluster leader computes control sequences for each agent in K according to the multiagent rollout algorithm with a greedy base heuristic using the assembled view information. These sequences are then broadcast throughout \mathcal{T}_K .

4. Execute Movement (EM): Each agent moves along its assigned trajectory, after which it unassigns itself from its cluster. If an agent does not belong to a cluster, it generates a random trajectory of bounded length and follows it.

We address each of these phases one at a time by presenting local algorithms that achieve the desired result. Note that DMAR is run by each agent individually, but all agents remain synchronized in their execution of DMAR. This is achieved by ensuring that each phase is executed using exactly the same number (a function of ψ) of operations regardless of which agent is performing the computation before continuing to the next phase. We also provide accompanying analysis that demonstrates that the local behavior we define achieves the collective goals outlined in Algorithm 1. All proofs for lemma and theorem statements can be found in Appendix A.

3.1 Self-organizing agent clusters (SOAC)

To achieve the desired clustering, agents for which tasks are currently visible form temporary cluster *centroids* via a local leader election scheme. Then, based on the size parameter ψ , the clusters gradually grow by iteratively appending nearby agents. At the start of SOAC, each agent sets an internal flag indicating whether it sees a task. Then, if an agent a sees a task while simultaneously seeing other agents that each see tasks as well, a disqualifies itself from becoming a centroid if any such agent has a larger ID value. Any remaining agents after the above process form centroids of new unique clusters. Next, SOAC iteratively appends agents to existing clusters over multiple PS time steps. There is a number of PS steps for each $i = 1, 2, \dots, \psi$. At iteration i , for any agent a that does not belong to a cluster, a searches its view for any agent a' that already belongs to a cluster (say K') and joins K' by becoming the child of a' . Consequently, as each cluster K grows, a bi-directional tree structure \mathcal{T}_K is maintained representing a restricted communication network for agents in cluster K . Moreover, each agent maintains a separate cluster ID obtained from their parent. This cluster ID originates from the centroid and is handed off to each subsequent agent that joins the cluster.

For clusters in close proximity to one another, SOAC employs a mechanism to combine them into larger clusters called *cluster-join*. This is motivated by the principle that communication between adjacent clusters generally leads to better solutions. For any agent a that is not a member of a cluster at iteration i , if a sees other agents a', a'' that are members of distinct clusters, agent a declares itself the centroid of a new, larger cluster that attempts to acquire all agents of clusters K', K'' corresponding to those of a' and a'' , respectively. This is achieved via propagation of a message throughout $\mathcal{T}_{K'}$ and $\mathcal{T}_{K''}$ that requests recipients to adopt the new centroid ID (that of agent a). This propagation mechanism works as follows: After an agent $b \in K' \cup K''$ propagates the message away from a neighboring sender s , it reconfigures its pointers such that its parent pointer now points to s , and a child pointer of s now points to b . Now b is a sender with respect to its remaining neighbors. If an agent receives multiple cluster reassignment messages simultaneously, it will disregard all but one chosen arbitrarily. Note that because of the possibility that an agent may receive multiple cluster reassignment requests simultaneously, not all agents of K', K'' may join the new larger cluster, since some may join other clusters in this manner. Only after these larger clusters are formed does SOAC continue to iteration $i + 1$. Each agent continues propagating messages for $\mathcal{O}(2^\psi)$ PS time steps per

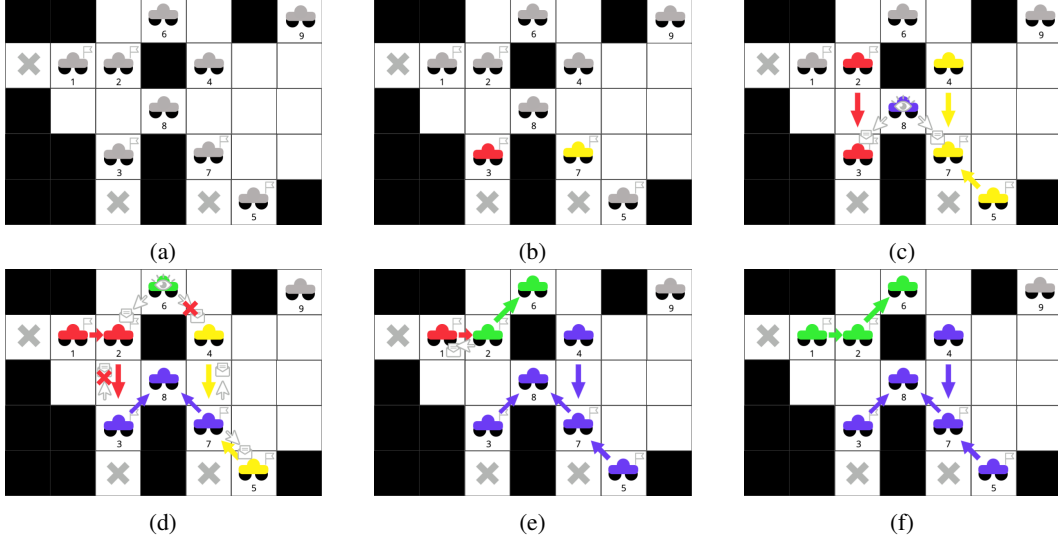


Figure 1: Example execution of SOAC. Car objects represent agents. Only white tiles are visitable. Gray crosses indicate task positions. Agent colors indicate cluster membership and gray agents belong to no cluster. IDs are indicated below each agent. Flags indicate which agents see tasks. Assume $k = \psi = 2$. (a) Agents initially belong to no cluster. Agents 1,2,3,5,7 see tasks. (b) Agents 1,2,5 see agents with larger IDs who see tasks, hence disqualify themselves. Agents 3,7 become centroids of new clusters. (c) Iteration 1 begins. Agents 2,4,5 join clusters, colored arrows indicate tree pointers. Agent 8 sees agents in different clusters and initiates a join with messages. (d) Agents 3,7 join the purple cluster, send messages to children to request reassignment. Agent 2 rejects request from 3 (as it received two messages at once). Agent 6 initiates cluster join, 4 rejects request. (e) Iteration 2 begins. Agent 2 joins the green cluster. Agent 4 favors the purple cluster, 5 joins the purple cluster as well. Agent 2 sends request to 1. (f) Agent 1 joins green cluster yielding final configuration. Agent 9 was too distant to join a cluster.

iteration. This allows a sufficient number of message requests to be passed for a join request to reach all agents in the tree (see Lemma 3.1). After $\mathcal{O}(\psi 2^\psi)$ PS time steps, the process yields a collection of clusters (and possibly some agents that belong to no clusters.) The number of agents per cluster is at most a constant since the number of children any parent can have is restricted to be a constant. If the would-be parent of an agent attempting to join a cluster has no available child pointers, then that agent simply does not join the cluster. We provide a visual example of a SOAC execution in Figure 1. The following lemma demonstrates SOAC correctly generates clusters and bounds the running time.

Lemma 3.1. *Let $K \subseteq S$ be an arbitrary cluster of agents in G obtained as a result of SOAC. Then, without violating locality restrictions, (i.) K forms a restricted communication network \mathcal{T}_K rooted at a centroid c and with height $\mathcal{O}(2^\psi)$, (ii.) all agents in \mathcal{T}_K associate their membership in K with c , (iii.) SOAC terminates in $\mathcal{O}(\psi 2^\psi)$ PS time steps.*

3.2 Local map aggregation (LMA)

At the end SOAC, a subset of the agents is organized into clusters, for each of which there exists a respective centroid. In the second phase, the objective is that for each independent cluster K with centroid c , agent c obtains a map of K , which reflects the collective view of the cluster ($\nu(K)$). At a high level, agents in K convey their internal representations of their views to their neighbors in their restricted communication network \mathcal{T}_K , and as these representations are collected, they build upon one another until c obtains a map of the entire cluster view.

An agent a possesses in memory a *map* structure $\mathcal{M}(a)$ that includes $\nu(a)$, as well as possibly the views of other agents (although initially $\mathcal{M}(a) = \nu(a)$). A *complete map* $\mathcal{M}(K)$ of a cluster K includes the union of views of every agent in K . For convenience, when we have two maps \mathcal{M} and \mathcal{M}' , we use the notation $\mathcal{M} \cup \mathcal{M}'$ to denote the component-wise unions of each map described above. Agent c will initiate the propagation of messages down to the leaves of \mathcal{T}_K (identifiable as

those agents with NULL child pointers.) After a sufficient number of PS time steps have passed, each leaf a sends $\mathcal{M}(a)$ to its respective parent b , who upon receiving $\mathcal{M}(a)$ will generate a new map $\mathcal{M}'(b) := \mathcal{M}(b) \cup \mathcal{M}(a)$. This process then iterates $\mathcal{O}(2^\psi)$ times from child to parent until c receives a complete map, i.e. $\mathcal{M}(c) = \mathcal{M}(K)$. Agents repeatedly propagate messages long enough for the height of the largest tree to be traversed twice (first down then up) by messages. Note that the number of messages passed from a parent to its children is constant since any agent has at most a constant number of children. Correctness and running time are guaranteed by the following lemma.

Lemma 3.2. *Given an agent tree \mathcal{T}_K , local map aggregation provides the centroid c of a cluster K with a complete map $\mathcal{M}(c) = \mathcal{M}(K)$ of K after $\mathcal{O}(2^\psi)$ PS time steps without violating locality restrictions.*

3.3 Team-restricted multiagent rollout (TMAR) and execute movement (EM)

TMAR describes how to apply multiagent rollout from [9] to an independent cluster K that does not violate the distance visibility restrictions on the agents in K . From the previous sections, it is clear that after the sequential execution of SOAC followed by LMA, each cluster K is structured as a spanning tree \mathcal{T}_K rooted at the centroid agent c , who possesses a complete map $\mathcal{M}(K)$. Agent c executes multiagent rollout on $\mathcal{M}(K)$ to obtain control sequences for each agent in K in the sequence given by ascending agent IDs. Agent c then initiates a broadcast of these sequences (via parent-to-child message passing in \mathcal{T}_K), each of which are associated with a specific agent ID. After enough iterations have passed for each agent to receive its corresponding control sequence, each agent will simply execute their respective control sequence via movement. To maintain synchronization between all clusters, each agent will wait an additional number of time steps until it reaches a maximum control sequence length $\lambda(\psi)$ —a function on ψ that returns the time required for a breadth-first search over K . For any agent a not in a cluster, instead of following a computed control sequence, a generates a random control sequence of length at most $\lambda(\psi)$ and executes this instead, thereby exploring the network. The sequence is generated by choosing successive vertices each uniformly at random from the neighborhood of the previous (this is precisely a random walk [20]). Correctness is guaranteed by the following lemma:

Lemma 3.3. *Each agent in a cluster K receives a control sequence Q^a according to multiagent rollout applied to $\mathcal{M}(K)$ within $\mathcal{O}(2^\psi)$ PS time steps, and executes Q^a within $\mathcal{O}(2^{2(\psi-1)}) = \mathcal{O}(1)$ PS time steps.*

As each of SOAC, LMA, TMAR and EM require a constant number of PS time steps to execute by Lemmas 3.1, 3.2, and 3.3, we obtain our primary theoretical result regarding DMAR for UMVRP-L:

Theorem 3.4. *Given a vehicle routing network $G = (V, E)$, a set S of m agents with constant maximum degree, and a set τ of task positions, then, without violating locality restrictions, an iteration of DMAR (i.) generates zero or more agent clusters; (ii.) provides that for each cluster K , every agent in K receives a control sequence according to multiagent rollout applied to $\mathcal{M}(K)$; and (iii.) each instance $\mathcal{M}(K)$ is solved in a constant number of PS time steps.*

4 Experimental results

4.1 Discrete-space simulations

We consider eight classes of instances of UMVRP-L; namely 10×10 , 20×20 , \dots , and 80×80 grids. For each class, we uniformly sample ten random connected topologies that include obstacles over 20% of the nodes. For each $n \times n$ grid, we consider a variety of different k -values, as well as three agent-to-task ratios; including 1:2, 1:1 and 2:1. Agents and tasks are distributed uniformly at random over each instance for each ratio, and the number of agents is always n . Moreover, we disregard any topology that contains geographically isolated tasks, i.e. where the worst-case expected length of a random walk to visit each task would be unreasonably large. For all simulations, we fixed $\psi = 3$. As our algorithms require random exploration, we run ten independent runs per instance. For each grid size and k -value combination, we report costs and runtime and number of clusters formed averaged over ten runs over ten instances for each of the three agent-to-task ratios. Due to time constraints, we only capture average cluster count information for the values corresponding to the extreme cases and the mean for each k value. In Appendix B, we provide additional runs with confidence intervals to further solidify these results. For each of these combinations we run DMAR and the base policy

(BP). Note that the base policy still performs SOAC and LMA, however TMAR is replaced by the greedy policy and as such there is no agent coordination. The combinations described above result in approximately 50,000 individual simulations over 5,000 instances. In this work we present results from 40×40 , 60×60 and 80×80 grids, but comprehensive results can be found in Appendix B.

We observe from Figure 2(a-c) that for each grid on $N = n \times n$ nodes there exists a critical radius $k^*(N)$ whereby for all $k \geq k^*(N)$, rollout outperforms the base policy. As k decreases, we see that the performance of rollout degrades gracefully; and as k increases, the total average running time seems to increase exponentially to account for increased online planning, illustrating the trade-off between scalability and solution quality. From Figure 2(a-f) we see that an effective range of radii exists wherein there exists a radius for which there are multiple clusters generated and the relative cost improvement is a factor of approximately two. At this radius we achieve a total running time that is a small fraction of the average time corresponding to the largest k values we considered. Note that the average running time for DMAR on an instance at any k value is no larger than the running time of the centralized multiagent rollout algorithm, hence the observed improvement in runtime represents a lower bound when comparing DMAR to the same. We note also that for k values considered beyond the effective range, we only observe a further constant factor relative cost improvement. In Figure 2(g), we plot an approximation $k^*(N)$ obtained from our sampling along with several other slow-growing functions. We see that $k^*(N)$ is closely approximated by $\log_2^*(N)$. Consequently, we mark our effective range bounds in Figure 2(a-f) (indicated by the shaded box) as $2\log_2^*(N)$ to $3\log_2^*(N)$ (or 8 to 12).

4.2 Physics-based simulations and robotics experiments

To address the question of whether DMAR is applicable to real-world scenarios, we have created an implementation that adapts DMAR to continuous space using the Robotarium platform [25]. Here, each agent is represented by a robot capable of local sensing, and can differentiate between other agents, obstacles and tasks. These simulations capture the dynamics of differential drive-based robots; that is, each robot’s movement is generated by actuation of motors, the dynamics of which are described by a set of ordinary differential equations. In this adaptation, planning by each robot is still considered in discrete space (9×9 grids), however, once a discrete control sequence is computed, each control is then mapped to a continuous space velocity vector, after which the new robot position is realized by the actuators. Measures were also taken to avoid collisions. While the computation for this experiment is executed on a centralized server, the distributed aspects of our model were simulated by restricting information where appropriate.

Due to the size constraints on the Robotarium arena, we limit our simulations to thirty randomly generated environments of $2\text{ m} \times 2\text{ m}$ in size, each with a varying number of tasks and seven agents (each roughly the size of a mobile phone). For each instance, we ran ten executions to obtain average costs (as exploration is still random). In addition, we also vary the sensing radius k as 20 cm, 40 cm, 60 cm, 80 cm and ∞ . For all simulations, we fixed $\psi = 2$. The results of these experiments are displayed in Figure 2(i) and represent a proof-of-concept. They demonstrate that rollout outperforms the base policy regardless of k , although, as in the discrete-space simulations, its performance degrades gracefully as k decreases. Moreover, we see that as the radius increases, the number of clusters decreases. Although we ran these physical simulations in silico, we have augmented these simulations by executing our algorithm on physical robots using aforementioned Robotarium platform on many instances, as demonstrated in Figure 2(h). A technical discussion about our approach to physics-based simulations and robotics is provided in Appendix C.

5 Conclusions and limitations

In this work we have presented a distributed computing approach for applying rollout to a generalization of the multivehicle routing problem whereby agents possess no a priori knowledge of the network on which they operate and possess limited local sensing capabilities. This study allowed us to examine the role of communication in rollout, and the effect limiting communication has on performance. Our approach produces quality solutions provided the local sensing radius is large enough, but it need not be so large that the collective views of agents cover the entire network. We have shown that there exists a critical sensing radius whereby there is sufficient local information available to agents so that rollout will outperform a less sophisticated myopic strategy for all larger radii. This critical radius is

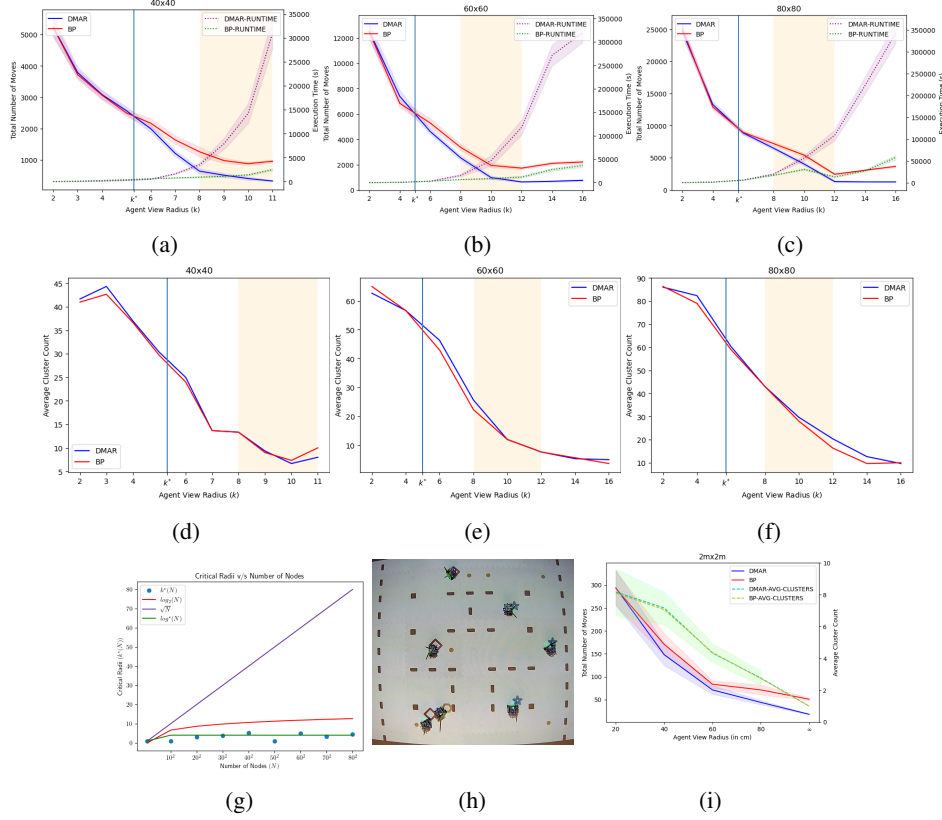


Figure 2: Experimental results. (a-c, left vertical axis) Discrete-space simulation plots show the average cost of the base policy (red curves) vs average cost of DMAR (blue curves) on 40×40 , 60×60 , and 80×80 grids. (a-c, right vertical axis). Curves correspond to average running time in seconds for both DMAR and the base policy. Critical radii are marked as k^* are marked, effective ranges are represented by the shaded orange boxes. (d-f) Plots show average number of clusters formed per run with critical radii and effective ranges likewise marked. (g) Sampled critical radii function $k^*(N)$ juxtaposed with other slow-growing functions. (h) DMAR execution in Robotarium [25]. Shapes (star, diamond, hexagon) correspond to separate clusters. Small circles represent tasks, and quadrilaterals represent obstacles. The robots represent agents. (i) Physics-based simulation proof-of-concept on $2\text{ m} \times 2\text{ m}$ environments. The left vertical axis corresponds to average solution cost, and the right axis corresponds to average number of clusters generated. 95% confidence intervals are given by shaded regions around their respective means.

bounded by a constant for all practical purposes. Moreover, there exists a range of effective radii (two to three times the critical radius) that contains radii for which communication is still significantly limited, but the relative cost improvement over the base policy is approximately a factor of two. We saw that for certain radii in this effective range, the running time of DMAR was exponentially smaller than for larger radii, with only a constant factor performance detriment to those of the largest radii we considered. This implies the superior scalability of our approach, and illustrates a trade-off between performance and the same. This also implies that the user may choose a radius between 8 and 12 and expect substantial relative cost improvement and fast execution without knowledge of the network size. Lastly, we have shown conceptually that our approach is adaptable to continuous space and robust to sensor noise, augmenting its real-world applicability.

Although we were able to simulate dozens of agents on networks with thousands of nodes, we used centralized computation to simulate distributed computation, which prevented us from considering even larger instances. Future work is necessary to evaluate performance on truly distributed systems, which may not necessarily reflect our rather strong synchronized clock assumption. Theoretical foundations for the critical sensing radius and the effective range are not present in our work currently, and the predictions we made regarding these objects is predicated on the experiments we ran.

Acknowledgment

Special thanks Ted Pavlic for guidance, Joseph Briones for simulation implementation support and Anya Chaturvedi for organizational support. Research partially supported under NSF CCF-1637393 and CCF-1733680 and DoD-ARO MURI No.W911NF-19-1-0233 awards.

References

- [1] Chris Amato, George Dimitri Konidaris, Leslie Pack Kaelbling, and Jonathan P. How. Modeling and planning with macro-actions in decentralized pomdps. *The journal of artificial intelligence research*, 64:817–859, 2019.
- [2] Christopher Amato, George Konidaris, Ariel Anders, Gabriel Cruz, Jonathan P How, and Leslie P Kaelbling. Policy search for multi-robot coordination under uncertainty. *Int. J. Rob. Res.*, 35(14):1760–1778, dec 2016.
- [3] Christopher Amato, George Konidaris, Gabriel Cruz, Christopher A. Maynor, Jonathan P. How, and Leslie P. Kaelbling. Planning for decentralized control of multiple robots under uncertainty. In *2015 IEEE International Conference on Robotics and Automation (ICRA)*, pages 1241–1248, 2015.
- [4] Dana Angluin, James Aspnes, Zoë Diamadi, Michael J. Fischer, and René Peralta. Computation in networks of passively mobile finite-state sensors. In *Proceedings of the Twenty-Third Annual ACM Symposium on Principles of Distributed Computing*, PODC ’04, page 290–299, New York, NY, USA, 2004. Association for Computing Machinery.
- [5] G Balamurugan, J Valarmathi, and V P S Naidu. Survey on uav navigation in gps denied environments. In *2016 International Conference on Signal Processing, Communication, Power and Embedded System (SCOPEs)*, pages 198–204, 2016.
- [6] Yoshua Bengio, Jérôme Louradour, Ronan Collobert, and Jason Weston. Curriculum learning. In *Proceedings of the 26th Annual International Conference on Machine Learning*, ICML ’09, page 41–48, New York, NY, USA, 2009. Association for Computing Machinery.
- [7] Daniel S. Bernstein, Shlomo Zilberstein, and Neil Immerman. The complexity of decentralized control of markov decision processes. In *Proceedings of the Sixteenth Conference on Uncertainty in Artificial Intelligence*, UAI’00, page 32–37, San Francisco, CA, USA, 2000. Morgan Kaufmann Publishers Inc.
- [8] Dimitri P. Bertsekas. *Dynamic Programming and Optimal Control*, volume 1. Athena Scientific, Belmont, Massachusetts, 4 edition, 2017.
- [9] Dimitri P. Bertsekas. *Rollout, Policy Iteration, and Distributed Reinforcement Learning*. Athena Scientific, Belmont, Massachusetts, 1 edition, 2020.
- [10] Dimitri P. Bertsekas and John N. Tsitsiklis. *Neuro-Dynamic Programming*. Athena Scientific, 1st edition, 1996.
- [11] Sushmita Bhattacharya, Siva Kailas, Sahil Badyal, Stephanie Gil, and Dimitri P. Bertsekas. Multiagent rollout and policy iteration for pomdp with application to multi-robot repair problems. In *4th Conference on Robot Learning*, Cambridge, Massachusetts, 2020.
- [12] G.S. Chirikjian. Kinematics of a metamorphic robotic system. In *Proceedings of the 1994 IEEE International Conference on Robotics and Automation*, pages 449–455 vol.1, 1994.
- [13] Floriano De Rango, Nunzia Palmieri, Xin She Yang, and Salvatore Marano. Bio-inspired exploring and recruiting tasks in a team of distributed robots over mined regions. In *2015 International Symposium on Performance Evaluation of Computer and Telecommunication Systems (SPECTS)*, pages 1–8, 2015.
- [14] Zahra Derakhshandeh, Shlomi Dolev, Robert Gmyr, Andréa W. Richa, Christian Scheideler, and Thim Strothmann. Amoebot - a new model for programmable matter. In *Proceedings of the 26th ACM Symposium on Parallelism in Algorithms and Architectures*, SPAA ’14, page 220–222, New York, NY, USA, 2014. Association for Computing Machinery.

- [15] Jakob N. Foerster, Gregory Farquhar, Triantafyllos Afouras, Nantas Nardelli, and Shimon Whiteson. Counterfactual multi-agent policy gradients. In *Proceedings of the Thirty-Second AAAI Conference on Artificial Intelligence and Thirtieth Innovative Applications of Artificial Intelligence Conference and Eighth AAAI Symposium on Educational Advances in Artificial Intelligence*, AAAI'18/IAAI'18/EAAI'18. AAAI Press, 2018.
- [16] M. R. Garey, D. S. Johnson, and R. Endre Tarjan. The planar hamiltonian circuit problem is np-complete. *SIAM Journal on Computing*, 5(4):704–714, 1976.
- [17] Bruce L. Golden, Attila A. Kovacs, and Edward A. Wasil. Chapter 14: Vehicle routing applications in disaster relief. In *Vehicle Routing*, MOS-SIAM Series on Optimization, pages 409–436. Society for Industrial and Applied Mathematics, 2014.
- [18] Jayesh K. Gupta, Maxim Egorov, and Mykel Kochenderfer. Cooperative multi-agent control using deep reinforcement learning. In Gita Sukthankar and Juan A. Rodriguez-Aguilar, editors, *Autonomous Agents and Multiagent Systems*, pages 66–83, Cham, 2017. Springer International Publishing.
- [19] Soumya Kar, José M. F. Moura, and H. Vincent Poor. QD -learning: A collaborative distributed strategy for multi-agent reinforcement learning through consensus + innovations. *IEEE Transactions on Signal Processing*, 61(7):1848–1862, 2013.
- [20] Rajeev Motwani and Prabhakar Raghavan. *Randomized Algorithms*. Cambridge University Press, 1995.
- [21] Stuart Russell and Peter Norvig. *Artificial Intelligence: A Modern Approach*. Prentice Hall Press, USA, 3rd edition, 2009.
- [22] Richard S Sutton and Andrew G Barto. *Reinforcement learning: An introduction*. MIT press, 2018.
- [23] Paolo Toth and Daniele Vigo. *The Vehicle Routing Problem. Monographs on Discrete Mathematics and Applications.*, volume 9. Philadelphia: Society for Industrial and Applied Mathematics, 2002.
- [24] J.E. Walter, E.M. Tsai, and N.M. Amato. Algorithms for fast concurrent reconfiguration of hexagonal metamorphic robots. *IEEE Transactions on Robotics*, 21(4):621–631, 2005.
- [25] Sean Wilson, Paul Glotfelter, Siddharth Mayya, Gennaro Notomista, Yousef Emam, Xiaoyi Cai, and Magnus Egerstedt. The robotarium: Automation of a remotely accessible, multi-robot testbed. *IEEE Robotics and Automation Letters*, 6(2):2922–2929, 2021.
- [26] Damien Woods, Ho-Lin Chen, Scott Goodfriend, Nadine Dabby, Erik Winfree, and Peng Yin. Active self-assembly of algorithmic shapes and patterns in polylogarithmic time. In *Proceedings of the 4th Conference on Innovations in Theoretical Computer Science*, ITCS '13, page 353–354, New York, NY, USA, 2013. Association for Computing Machinery.
- [27] Mark Yim, Wei-min Shen, Behnam Salemi, Daniela Rus, Mark Moll, Hod Lipson, Eric Klavins, and Gregory S. Chirikjian. Modular self-reconfigurable robot systems [grand challenges of robotics]. *IEEE Robotics and Automation Magazine*, 14(1):43–52, 2007.

A Technical arguments

A.1 Proof of Lemma 3.1

Proof. (i.) can be argued from the fact that clusters are defined by the tree structure of the restricted communication network. Each tree is formed around a single centroid with a parent pointer set to NULL. Agents append themselves as leaves layer by layer to a single parent, and hence cannot form a cycle. Upon appending as a leaf, an agent will adopt the cluster ID of its parent, which can inductively be traced back to c . In the cluster-join process, the parent pointer of an agent a will always point to the agent from which it received (and accepted) a request, which can likewise be traced back to the initiating centroid. As agent a removes its child pointers after propagating the request, it becomes a leaf of the new tree, and therefore any of its former children will undergo the same process to join the new tree. The height of \mathcal{T}_K is dependant on ψ . Arguing by induction on the loop iteration i , it's easy to see that the size of a cluster at most doubles at any iteration (plus one for the joining agent) since the total number of agents cannot exceed a constant. Solving the corresponding recurrence relation yields a height bound of $\mathcal{O}(2^\psi)$. Hence waiting $\mathcal{O}(2^\psi)$ PS time steps per iteration is enough time for messages to propagate through the largest tree, and so all agents in \mathcal{T}_K will agree on the centroid ID, implying (ii.). Lastly, (iii.) follows from simple counting. \square

A.2 Proof of Lemma 3.2

Proof. By Lemma 3.1, the maximum height of \mathcal{T}_K is $\mathcal{O}(2^\psi)$. It is then clear from Algorithm 1 that $\mathcal{O}(2^\psi)$ is a sufficient number of PS time steps so that the leaves of \mathcal{T}_K receive partial cluster maps from centroid c . Likewise, broadcasts of partial map information from the farthest leaf to the root requires at most $\mathcal{O}(2^\psi)$ PS time steps, hence after exactly $\mathcal{O}(2^\psi)$ PS time steps, agent c possesses a complete map of \mathcal{T}_K . By the labelling scheme giving in Algorithm 4, the complete map obtained by centroid c is labelled with coordinates relative to $\rho(c) = (0, 0)$. This follows since the map originates from the centroid, where it is labelled with relative coordinates to $\rho(c) = (0, 0)$, and every map union operation appends to nodes to a partial map that contains the original map of c , hence the relative labelling scheme is preserved in the complete map. \square

A.3 Proof of Lemma 3.3

Proof. By Lemma 3.1 and Algorithm 1, each agent obtains its control sequence within $\mathcal{O}(2^\psi)$ PS time steps and simply moves accordingly. By Lemma 3.1, the diameter of \mathcal{T}_K is bounded by $\mathcal{O}(2^\psi)$, hence $\lambda(\psi) = \mathcal{O}(2^{2(\psi-1)})$ since the runtime of BFS is asymptotically linear when the maximum degree is constant. This bound is sufficiently large since, in the worst case, a greedy policy would cause each agent to visit every node in $\mathcal{M}(K)$ (if each agent always moved toward the same task), and if there is a task at each node, the greedy policy precisely produces a breadth-first search (as the edges are not weighted). Since the base policy is greedy and multiagent rollout has cost-improvement guarantees for greedy base policies; i.e. it can perform no worse than the base policy [9], multiagent rollout can never produce a trajectory longer than $\lambda(\psi)$. As each agent spends $\mathcal{O}(2^\psi)$ PS time steps in TMAR, and exactly $\lambda(\psi)$ PS time steps in EM, these phases terminate in $\mathcal{O}(2^{2(\psi-1)})$ PS time steps. \square

A.4 DMAR variant with enforced cost-improvement property

In this section we present a modification of DMAR (and its corresponding base policy) that contain additional mechanisms that guarantee cost improvement—although at a cost. This is motivated by the fact that global solution quality is dependent on the sequence of clusters formed, and therefore cost improvement obtained from solving clusters using DMAR can be difficult to measure.

We present a modified version of DMAR with a guaranteed relative cost-improvement property (DMAR-GCI), whereby after all tasks in a cluster K are completed, the agents of K gather at a common position within the cluster view (known as a *depot*) regardless of whether rollout or the base policy (denoted as BP-GCI) is being executed. More specifically, let Q be the set of control sequences for K computed by the centroid agent c during an execution of TMAR. Also, denote $\rho_f(Q^a)$ as the final position of agent a as obtained from executing the control sequence Q^a . Agent c then chooses a cluster depot at its own final position (i.e. $\rho(c)$) and appends additional movements to

each control sequence such that for each agent $a \in K$, the control sequence corresponding to the shortest path from $\rho_f(Q^a)$ to $\rho(c)$ is appended to the end of Q^a (followed by the required number of WAIT controls; see Appendix D). Agent c then initiates the broadcast of Q as normal. As such, the final position of all agents in K is necessarily $\rho(c)$. In this scheme we also prevent exploring agents from interfering with existing clusters. If an agent $a \in K$ is visiting a task location $v \in \nu(K)$, agent a leaves a special “token” at v . If then v appears in the view of an agent $a' \notin K$, a' will still recognize v as a task location and treat it as such (even though visiting v does not increase the number of completed tasks). We refer to this as the *token mechanism*.

The following theorem specifies a cost-improvement guarantee for DMAR-GCI, and relies on the cost-improvement properties of multiagent rollout [9].

Theorem A.1. *For any instance I of UMVRP-L, the total cost generated by DMAR-GCI from an execution on I is no larger than the total cost generated by an execution of BP-GCI on I .*

Proof. We claim by induction on the number of iterations of DMAR-GCI/BP-GCI that under an identical source of randomness, parallel executions of DMAR-GCI and BP-GCI yield identical clustering sequences. We demonstrate the following invariant: Under an identical source of randomness, at the end of each iteration of DMAR-GCI/BP-GCI, each individual agent occupies the same respective node in both executions. As the source of randomness is common, the initial clusters formed will be identical in both executions. Moreover, at the end of the first iteration, the positions of all agents that are members of clusters will be the same in both executions, as all such agents will be gathered at their respective depots. By the token mechanism, each agent that is not a member of a cluster will also end the first iteration of DMAR-GCI/BP-GCI in the same location in both instances, as differences in the order in which BP-GCI and DMAR-GCI complete tasks will not influence the trajectories of exploring agents. Hence, in both executions, each agent occupies the same respective position at the end of the first iteration. For an arbitrary iteration, if we assume agents occupy the same respective positions in both runs of DMAR-GCI/BP-GCI, then an analogous argument demonstrates that the invariant holds for the next iteration, as the initial agent positions are arbitrary and identical in both executions.

The policy generated by BP-GCI for each agent is given by its movement sequences, which are a combination of random exploration movements, as well as movements within clusters dictated by the greedy base policy. As these random movements are identical regardless of whether generated by DMAR-GCI and BP-GCI, and the greedy base policy applied within a cluster is *sequentially consistent* (i.e. from one stage to the next, the base policy does not deviate; see [9]), BP-GCI is also a sequentially consistent base policy for DMAR-GCI. From [9], this property suffices to conclude that DMAR-GCI can perform no worse than BP-GCI. \square

As the exploration costs are identical between DMAR-GCI and BP-GCI, they can be discounted, and hence we may directly compare the performance of our rollout scheme to the base policy without accounting for exploration. Note that DMAR-GCI is purely an analytical tool that is not meant to be used in practice. Its purpose is to allow us to compare DMAR with the base policy directly, without accounting for volatile random exploration. In Appendix B, we show that DMAR-GCI approximates DMAR (overhead is added for agents congregating at the depots), and hence the DMAR-GCI versus BP-GCI comparison may provide a better sense of the cost-improvement effect of DMAR for UMVRP-L.

B Additional simulation results

The full results (i.e. for each grid size $10 \times 10, 20 \times 20, \dots, 80 \times 80$) from comparing the average total costs generated by both DMAR and BP, as well as the corresponding average runtimes are presented in Figure 3. These results fall in line with the analysis given in Section 4.1; that is, the critical radius is approximately 4, and the effective region is between $k = 8$ and $k = 12$, wherein there exists a radius for which we observe an approximate 2-factor relative cost improvement. Moreover, beyond the effective range, the running time of DMAR increases seemingly exponentially. The only exceptions are the 10×10 grids, where DMAR outperforms the base policy for all radii tested on average. However, these small instances do not represent the trends we find from scaling the instances. In Figure 4, we present the average cluster counts for both DMAR and BP for $20 \times 20, 40 \times 40, 60 \times 60$ and 80×80 grid sizes. This figure differs from Figure 2(d-f) in that it represents the average number

of clusters over the majority of the instances we generated, and hence there are sufficient data to compute 95% confidence intervals (included in the plots). We see that in the effective region, the average number of clusters is still non-zero on average, implying communication is still limited for these k -values.

B.1 Simulation results for DMAR-GCI

In Figure 5, we present the results for comparing the average total costs of DMAR-GCI and BP-GCI. Each data point (k -value for a specific grid size) is an average of 50 or more individual simulations over various topologies and agent-to-task ratios. We validate Theorem A.1 by observing that the average total costs obtained from DMAR-GCI are no larger than those of BP-GCI for any k -value or grid size considered. We see that in comparison to DMAR (Figure 3), the average costs generated by DMAR-GCI are slightly larger than those generated by DMAR, although this difference becomes less pronounced as the grid size increases. We also observe that the proportion of total average cost attributed to random exploration moves is identical for both algorithms. Consequently, in Figure 6, we present the results from Figure 5 with the exploration costs subtracted out. As a result, the costs appear to increase with increasing k , although this is only due to the fact that the proportion of average total cost attributed to random exploration decreases with k (since more of the environment is visible to agents). Nevertheless, in the effective range ($k = 8$ to $k = 12$) and for each grid size, there exists a radius for which we observe a cost improvement factor between 1.7 and 2. As DMAR-GCI approximates the costs generated by DMAR, we cite DMAR-GCI to further support the cost-improvement claims with respect to DMAR.

C Experimental methods: robotics specifications

Each robot in the Robotarium is approximately $11\text{ cm} \times 10\text{ cm}$ and operates in an arena (Robotarium testbed) of $3\text{ m} \times 2\text{ m}$. The robots are initialized in the arena in accordance to the Cartesian coordinate plane with center of the arena being the origin of the plane. To transform the discrete-space version of DMAR to a continuous setting, we have approximated the arena (of size $2\text{ m} \times 2\text{ m}$) as a 9×9 grid of cells with each cell of size $20\text{ cm} \times 20\text{ cm}$. Robots do not strictly move as per the grid, but only use the center points of each cell as a guiding point when planning and moving. The actual motion of the robots is controlled using a hybrid controller, which first moves the robot on a linear path towards the goal position and then changes its orientation by rotating once at the goal position to point it in the desired direction. This provides for a smooth motion and allows for movement where robots can move past each other easily. The robots are based on a differential drive model and use single integrator dynamics to define a controller for the robot. The exact derivation and treatment of the robot dynamics are given in [25]. These dynamics incorporate robust barrier functions that ensure that inter-robot and wall-robot collisions do not occur.

For the simulations to function on actual physical robots, two important requirements arise that the DMAR algorithm must address:

1. **Collision barriers:** agents may not physically bump into each other while moving around in the arena.
2. **Collision avoidance:** no agent occupies the same space as another.

The barrier functions of the Robotarium platform keep the physical robots safe from damage, hence this requirement is met. Now, unlike the discrete simulations where robots may occupy the same location at a given time on the grid space, in a physical environment, two robots cannot occupy the same space at a given time. This required the use of a collision avoidance mechanism, which we have designed to be least obtrusive to the original algorithm’s movement decisions (described below).

All the phases of the Algorithm 1 progress as before, except we augment the last phase of Execute Movement. The mechanism deployed to achieve collision avoidance is described in Algorithm 2. Note that although the implementation is presented in a centralized fashion, an equivalent decentralized execution scheme exists using message passing between neighboring agents since all information used is local. The mechanism maintains the locality constraints and is based only on the assumptions that each agent is able to communicate freely with another agent within a fixed radius.

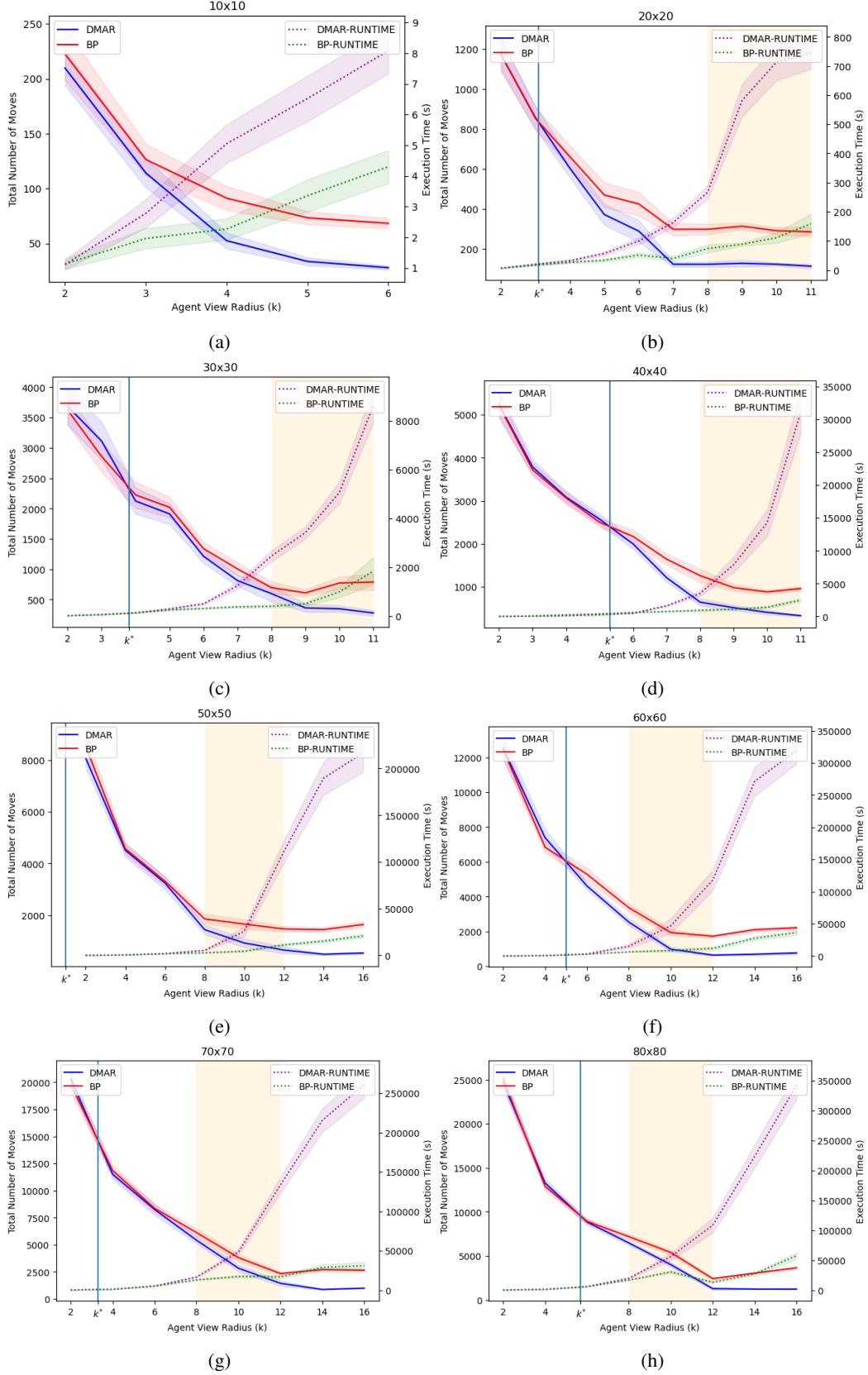


Figure 3: Experimental results. (a-h, left vertical axis) Discrete-space simulation plots show the average cost of the base policy (red curves) vs average cost of DMAR (blue curves) on 10×10 , 20×20 , \dots , 80×80 grids. (a-h, right vertical axis). Curves correspond to average running time in seconds for both DMAR and the base policy. Critical radii are marked as k^* , effective ranges are represented by the shaded orange boxes. 95% confidence intervals are given by shaded regions around their respective means.

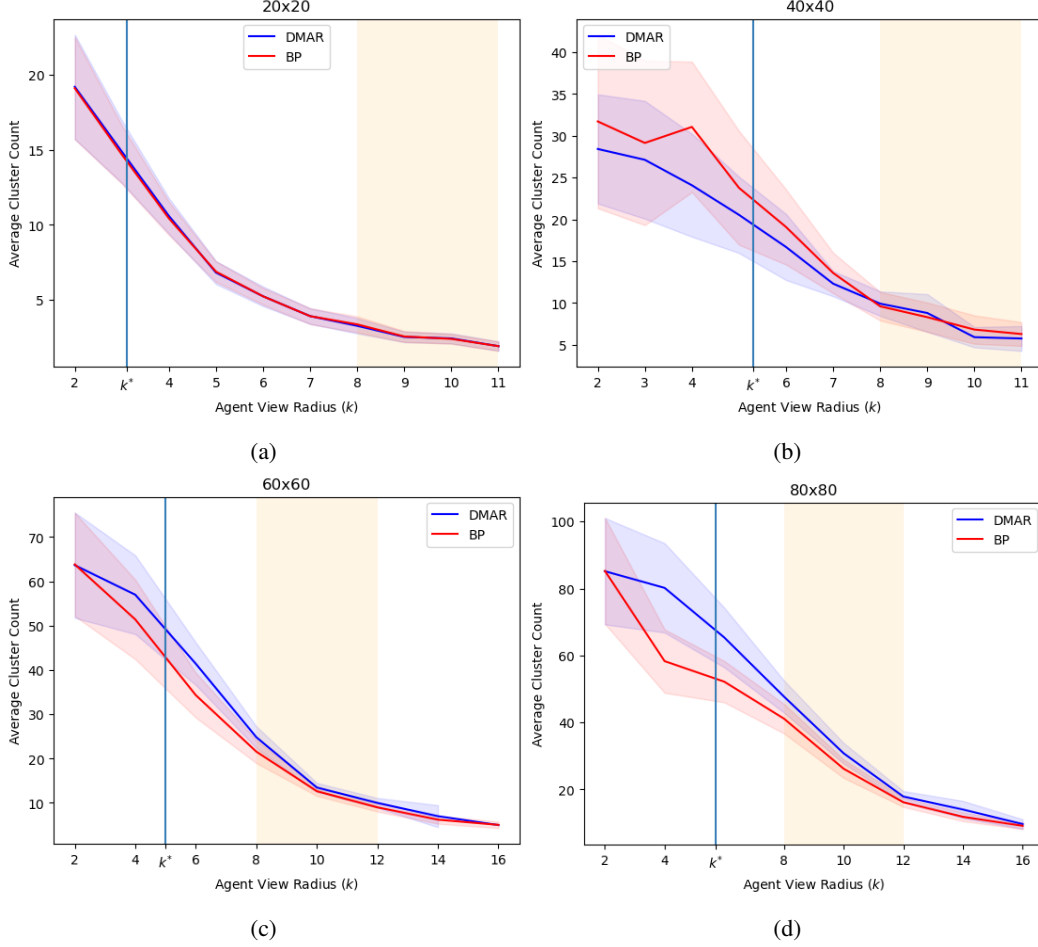


Figure 4: Discrete-space simulation plots show the average number of clusters generated by the base policy (red curves) vs average number of clusters generated by DMAR (blue curves) on 20×20 , 40×40 , 60×60 , and 80×80 grids. 95% confidence intervals are given as the shaded regions around their respective means. Critical radii are marked as k^* are marked, effective ranges are represented by the shaded orange boxes.

D Algorithm pseudocode

In this section, we provide pseudocode for each of the four phases of DMAR (SOAC, LMA, and TMAR and EM). These are found in Algorithms 3, 4, and 5, respectively. Loops are presented in terms of asymptotic functions of ψ , however, the asymptotic function $\mathcal{O}(f(\psi))$ can be replaced by $r \cdot f(\psi)$, where r is a sufficiently large constant. Each agent a possesses a set of modifiable attributes as follows:

1. A unique, immutable ID $a.ID$
2. A parent pointer $a.parent$, initialized to NULL.
3. A set of child pointers $a.children$, initialized to the empty set.
4. A set of indicators $a.clusters$ that describes the IDs of the cluster to which a belongs. This is initialized to the empty set.
5. A boolean flag $a.message$ indicating whether a has a message to pass.

¹Any added wait moves inserted are not accounted and any move's cost that is circumvented by moving forward in an agent's trajectory is accounted for to maintain the algorithm's cost integrity with the discrete implementation.

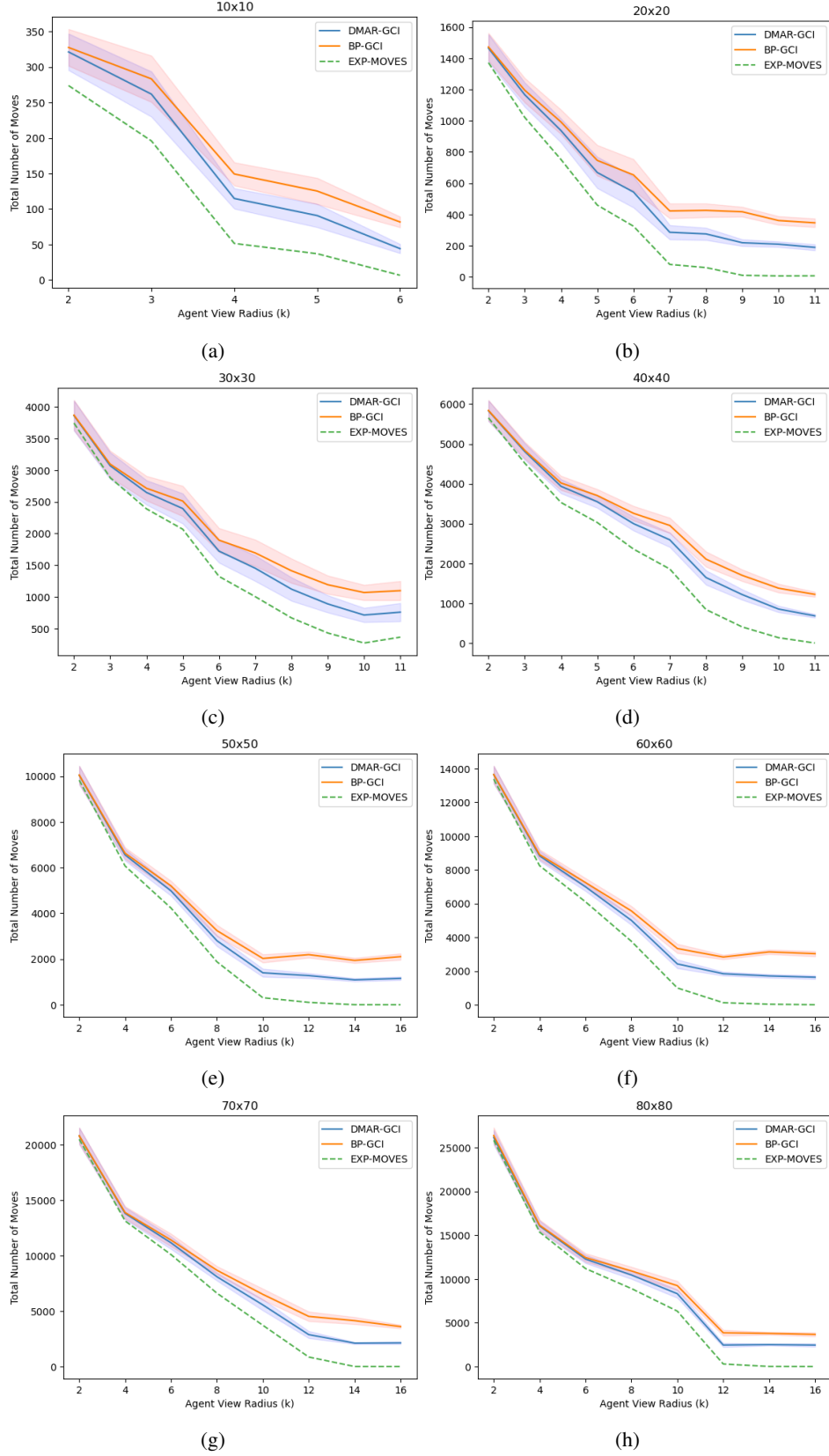


Figure 5: Experimental results. Discrete-space simulation plots show the average cost of BP-GCI (red curves) vs average cost of DMAR-GCI (blue curves) on 10×10 , 20×20 , ..., 80×80 grids. The green dashed curve represents the proportion of total cost that is attributed to exploration moves. This is identical for both algorithms. 95% confidence intervals are given by shaded regions around their respective means.

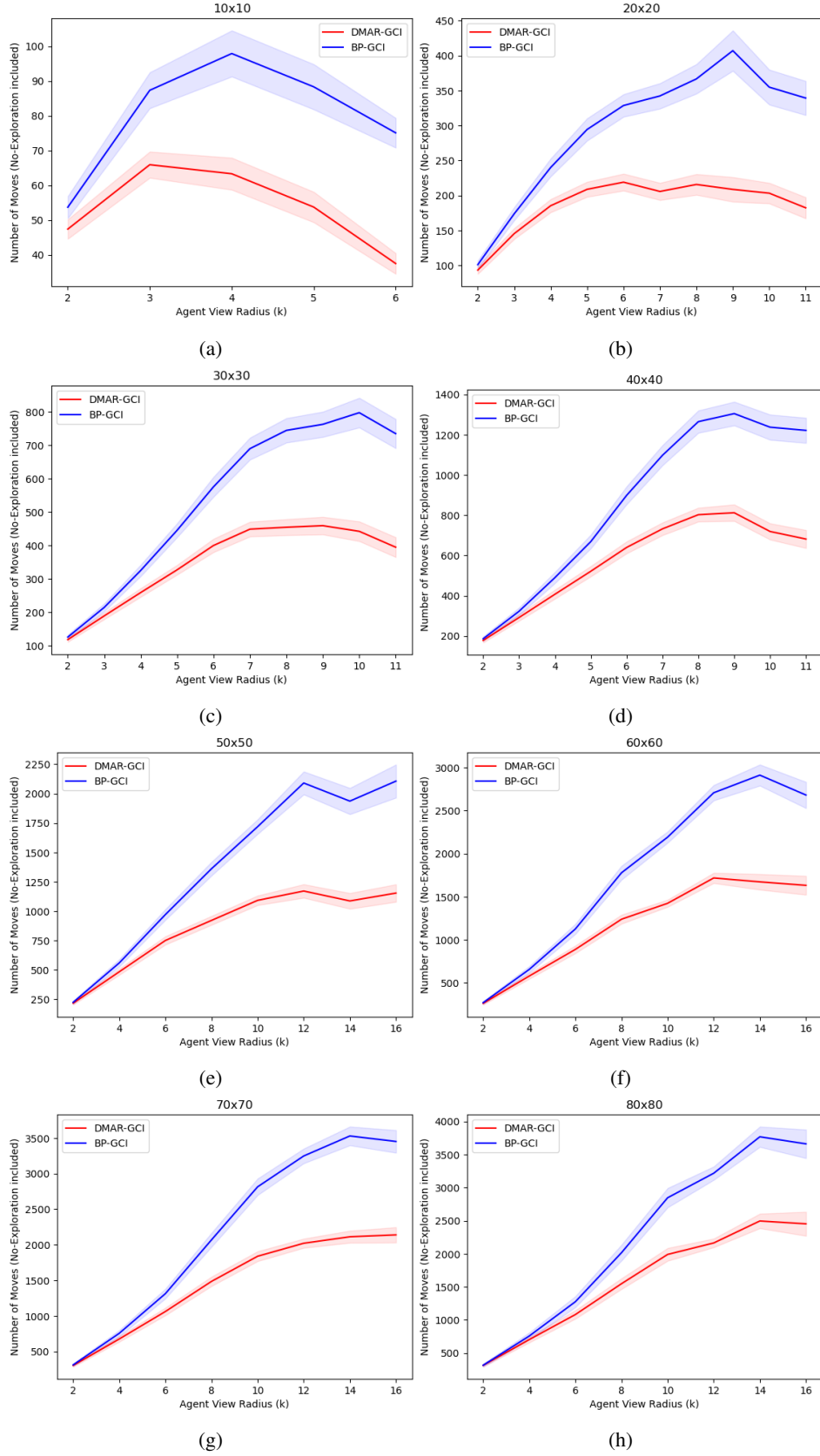


Figure 6: Experimental results. Discrete-space simulation plots show the average cost of BP-GCI (red curves) vs average cost of DMAR-GCI (blue curves) on 10×10 , 20×20 , ..., 80×80 grids. The common exploration cost incurred by both algorithms has been subtracted out. 95% confidence intervals are given by shaded regions around their respective means.

Algorithm 2 Collision Avoidance for continuous space DMAR

repeat until all agents have executed their control sequences

1. Locate Waiting Agents: Locate and note positions of agents that are exploring but have found a near-by task and are therefore waiting.

2. Detect Collisions: Execute a single move for each agent that is in a cluster and has remaining moves to execute. After performing a single move for each such agent, there may exist locations where there are two or more agents trying to occupy the same position (collisions).

while there exist collisions **do**

3. Define Precedence: For each collision, we define a priority order and decide which agent continues to the new location ℓ and which agent must remain at their previous location. Agents for whom ℓ is the final position (i.e. no additional moves remain in the control sequence or only WAIT moves remain), or those agents that are already waiting at ℓ are given preference.

4. Backtrack or Move ahead: Agents with remaining moves are considered for movement away from the collision location by consulting their respective control sequences. This is done iteratively by finding next position for the agent (a trajectory is created one step at a time according to computed controls) until a location which is collision-free(safe) is found. If a safe location is found then the agent directly moves to that location, circumventing any resulting locations in between. If a safe location is not found, then the agent will simply wait at its original position for a specified amount of time.

5. Deciding how long to Wait: Now there are two scenarios to consider: (1.) a safe location may open in future for the agent that has backtracked, or (2.) there is no chance of any safe location in the trajectory in the future. In scenario (1.), the agent simply backtracks with a wait move and will try to execute its move again before the end of the current DMAR iteration. In scenario (2.), the agent will backtrack and call that location its final position. These scenarios can be determined by each agent from examination of the complete set of control sequences given.

end while

6. Move Exploring Agents: Exploring agents take lowest precedent. If an exploring agent would make a random move that results in a collision, the agent backtracks and chooses another random move. The agent will simply wait if all potential moves result in a collision.

6. A control set $\{\text{NORTH, EAST, SOUTH, WEST, WAIT}\}$ containing possible directions in which an agent may move.
7. a task vertex pointer $a.\text{seesTasks}$ indicating that position of a task vertex in $\nu_t(a)$. This variable is initialized to NULL.
8. An internal representation of its local environment called a *map*. Let $G' = (V', E')$ be a graph isomorphic to G with some possibly different node labelling scheme. A map is a 3-tuple $a.\mathcal{M} = (a.\Gamma, a.\Phi, a.\Pi)$, where $a.\Gamma = (a.H, a.F)$ is a graph with $a.H \subseteq V'$ and $a.F \subseteq E$; $a.\Phi = (a.L, a.D)$ is a set of agent location and ID pairs with $a.L \subseteq V'$ and $a.D \subseteq S$; and $a.\Pi \subseteq V'$ is a set of task locations. This structure is initialized as $((\emptyset, \emptyset), (\emptyset, \emptyset), \emptyset)$.
9. A set $a.Q$ of control sequences, which is represented by a dictionary (keys reflect agent IDs); initialized to \emptyset .

We reference the function $\text{MULTIAGENTROLLOUT}(\mathcal{M})$, which takes a map \mathcal{M} and returns a set of control sequences Q as computed by the multiagent rollout algorithm from [9].

E Compute specifications

We used two sources of compute for our experiments:

1. Traditional x86 compute nodes were used which contain two Intel Xeon E5-2680 v4 CPUs running at 2.40GHz with at least 128 GB of RAM. There are 28 high speed Broadwell class CPU cores per node. The operating system is CentOS Linux 7 (Core), Kernel: Linux 3.10.0-693.21.1.el7.x86_64, Architecture: x86-64.

Algorithm 3 Self Organizing Agent Clusters Protocol for Agent a

```
1: if Agent  $a$  sees a task  $y$  in  $\nu(a)$  then
2:   Set  $a.seesTasks \leftarrow y$ 
   // leader election
3: if  $a.seesTask \neq \text{NULL}$  then
4:   Search  $\nu(a)$  for all agents  $x$  where  $x.seesTasks = a.seesTask$ 
5:   if  $x$  exists and  $a.ID > x.ID$  then
6:     Set  $a.seesTask \leftarrow \text{NULL}$ 
7:   if  $a.seesTask \neq \text{NULL}$  then
8:     Set  $a.cluster \leftarrow \{a.ID\}$ 
9:     Set  $a.parent \leftarrow \text{NULL}$ 
10: for  $i = 1, 2, \dots, \psi$  do
11:   if  $a.cluster = \emptyset$  then
12:     Search each agent  $x \in \nu(a)$ 
13:     if  $x.cluster \neq \emptyset$  then
14:       Set  $a.cluster \leftarrow a.cluster \cup \{x.ID\}$ 
15:       Set  $a.parent \leftarrow x$ 
16:       Set  $x.children \leftarrow x.children \cup \{a\}$ 
17:   if  $|a.cluster| > 1$  then
   // initiate cluster-join; agent in more than one cluster
18:   Set  $a.cluster \leftarrow \{a.ID\}$ 
19:   Set  $a.message \leftarrow \text{TRUE}$ 
20:   Set  $a.parent \leftarrow \text{NULL}$ 
21:   for each agent  $x \in \nu(a)$  where  $x.message = \text{FALSE}$  do
22:     Set  $x.cluster \leftarrow \{a.ID\}$ 
23:     Set  $x.message = \text{TRUE}$ 
24:     Set  $x.parent \leftarrow a$ 
25:     Set  $a.children \leftarrow a.children \cup \{x\}$ 
26:     Set  $x.children \leftarrow \emptyset$ 
27:   for  $j = 2, 3, \dots, \mathcal{O}(2^\psi)$  do
28:     if  $a.message = \text{True}$  then
29:       for all  $x \in \nu(a)$  where  $x.message = \text{FALSE}$  do
30:         Set  $x.cluster \leftarrow a.cluster$ 
31:         Set  $x.message \leftarrow \text{TRUE}$ 
32:         Set  $x.parent \leftarrow a$ 
33:         Set  $a.children \leftarrow a.children \cup \{x\}$ 
34:         Set  $x.children \leftarrow \emptyset$ 
35:   Set  $a.message \leftarrow \text{FALSE}$ 
```

2. A single compute node with AMD Ryzen 9 7950X Processor with 16 cores and 32 threads along with 64 GB of RAM. Physics based countinuous space simulations were exclusively run on this node. The operating system is Ubuntu 22.04.2 LTS, Kernel: Linux 6.2.0-76060200-generic, Architecture: x86-64.

F External links

Simulation animations and relevant captured footage from Robotarium can be found [here](#). Source code can be found [here](#).

Algorithm 4 Local Map Aggregation Protocol for Agent a

```
1: if  $a.parent = \text{NULL}$  and  $a.clusters \neq \emptyset$  then
2:   Let  $\nu_t(a) = (h_t(a), f_t(a))$ , be the view of  $a$  at time  $t$ 
3:   Let  $\phi_t(a) = (\ell_t(a), d_t(a))$  be the agent locations visible to  $a$  at time  $t$ .
4:   Let  $\pi_t(a)$  be task locations visible to  $a$  at time  $t$ 
5:   Set  $a.H \leftarrow a.H \cup h_t(a)$ ,  $a.F \leftarrow a.F \cup f_t(a)$ ,  $a.L \leftarrow a.L \cup \ell_t(a)$ ,  $a.D \leftarrow a.D \cup d_t(a)$ , and
    $a.\Pi \leftarrow a.\Pi \cup \pi_t(a)$ 
6:   Label all positions in the previous step relative to  $\rho_t(a) = (0, 0)$ .
7:   for  $b$  in  $a.children$  do
8:     Set  $b.H \leftarrow a.H$ ,  $b.F \leftarrow a.F$ ,  $b.L \leftarrow a.L$ ,  $b.D \leftarrow a.D$ ,  $b.\Pi \leftarrow a.\Pi$ 
9:   Set  $a.message \leftarrow \text{TRUE}$ 
   // propagate signal down the tree
10: for  $i = 1, 2, \dots, \mathcal{O}(2^\psi)$  do
11:   if  $a.parent \neq \text{NULL}$  and  $a.parent.message = \text{TRUE}$  then
12:     Let  $\nu_t(a) = (h_t(a), f_t(a))$ , be the view of  $a$  at time  $t$ 
13:     Let  $\phi_t(a) = (\ell_t(a), d_t(a))$  be the agent locations visible to  $a$  at time  $t$ .
14:     Let  $\pi_t(a)$  be task locations visible to  $a$  at time  $t$ 
15:     Set  $a.H \leftarrow a.H \cup h_t(a)$ ,  $a.F \leftarrow a.F \cup f_t(a)$ ,  $a.L \leftarrow a.L \cup \ell_t(a)$ ,  $a.D \leftarrow a.D \cup d_t(a)$ ,
     and  $a.\Pi \leftarrow a.\Pi \cup \pi_t(a)$ 
16:     Label all positions in the previous step relative to  $\rho_t(a.parent)$ .
17:     for  $b$  in  $a.children$  do
18:       Set  $b.H \leftarrow a.H$ ,  $b.F \leftarrow a.F$ ,  $b.L \leftarrow a.L$ ,  $b.D \leftarrow a.D$ ,  $b.\Pi \leftarrow a.\Pi$ 
19:     Set  $a.message \leftarrow \text{TRUE}$ 
   // propagate maps up the tree
20: for  $i = 1, 2, \dots, \mathcal{O}(2^\psi)$  do
21:   if  $a.parent \neq \text{NULL}$  then
22:     Set  $a.parent.H \leftarrow a.parent.H \cup a.H$ ,  $a.parent.F \leftarrow a.parent.F \cup a.F$ ,
        $a.parent.L \leftarrow a.parent.L \cup a.L$ ,  $a.parent.D \leftarrow a.parent.D \cup a.D$ ,
        $a.parent.\Pi \leftarrow a.parent.\Pi \cup a.\Pi$ 
```

Algorithm 5 Team-Restricted MA Rollout and Execute Movement Protocol for Agent a

```
   // TMAR
1: if  $a.parent = \text{NULL}$  and  $a.cluster \neq \emptyset$  then
2:   Compute  $a.Q \leftarrow \text{MULTIAGENTROLLOUT}(a.\mathcal{M})$ 
3:   Repeatedly append WAIT to each  $q \in a.Q$  such that  $|q| = \mathcal{O}(2^{2(\psi-1)})$ 
4: for  $i = 1, 2, \dots, \mathcal{O}(2^\psi)$  do
5:   for each  $x \in a.children$  do
6:     if  $x.Q \neq a.Q$  then
7:        $x.Q \leftarrow a.Q$ 
   // EM
8: if  $a.clusters = \emptyset$  then
9:   Set  $a.Q^{a.ID}$  to a sequence of  $\mathcal{O}(2^{2(\psi-1)})$  controls, each selected uniformly at random
10: Move according to  $a.Q^{a.ID}$ 
11: Re-initialize all variables
```
